



HAL
open science

Efficient blocking of planar defects by prismatic stacking faults in semipolar (112-2)-GaN layers on m-sapphire by epitaxial lateral overgrowth

B. Lacroix, M P Chauvat, P. Ruterana, G. Nataf, P. de Mierry

► **To cite this version:**

B. Lacroix, M P Chauvat, P. Ruterana, G. Nataf, P. de Mierry. Efficient blocking of planar defects by prismatic stacking faults in semipolar (112-2)-GaN layers on m-sapphire by epitaxial lateral overgrowth. Applied Physics Letters, 2011, 98, pp.121916. 10.1063/1.3571455 . hal-04706724

HAL Id: hal-04706724

<https://hal.science/hal-04706724v1>

Submitted on 23 Sep 2024

HAL is a multi-disciplinary open access archive for the deposit and dissemination of scientific research documents, whether they are published or not. The documents may come from teaching and research institutions in France or abroad, or from public or private research centers.

L'archive ouverte pluridisciplinaire **HAL**, est destinée au dépôt et à la diffusion de documents scientifiques de niveau recherche, publiés ou non, émanant des établissements d'enseignement et de recherche français ou étrangers, des laboratoires publics ou privés.

Efficient blocking of planar defects by prismatic stacking faults in semipolar (11 $\bar{2}$ 2)-GaN layers on m-sapphire by epitaxial lateral overgrowth

B. Lacroix,^{1,a)} M. P. Chauvat,¹ P. Ruterana,¹ G. Nataf,² and P. de Mierry²¹CIMAP, UMR 6252, CNRS-ENSICAEN-CEA-UCBN, 6 Bd Maréchal Juin, 14050 Caen, France²CRHEA, UPR 10, 1 rue Bernard Grégory, Sophia Antipolis, 06560 Valbonne, France

(Received 4 February 2011; accepted 7 March 2011; published online 25 March 2011)

For the next-generation solid state lighting, the production of high quality semipolar (11 $\bar{2}$ 2) GaN layers on sapphire obtained using asymmetric epitaxial lateral overgrowth (ELO) method has been investigated. This type of ELO leads to efficient blocking of the basal stacking faults (BSFs) in the bulk, and enables the formation of nondefective layers at the surface. The BSFs terminate due to generation of prismatic stacking faults along a well defined boundary. The corresponding intensity of GaN band edge photoluminescence emission is increased by more than four orders of magnitude in comparison to that from semipolar templates. © 2011 American Institute of Physics.

[doi:10.1063/1.3571455]

Nitride III-V semiconductors exhibit a wide range of band gap energies, which offer the possibility to cover all the visible spectral range for optical applications. Among them, gallium nitride (GaN) is now largely employed in the fabrication of light emitting diodes.¹ Until recently, these materials were mostly grown along the [0001] direction which leads to both spontaneous and piezoelectric polarization at interfaces.^{2,3} Such internal electric fields degrade the performance of optoelectronic devices, because they give rise to the quantum confined Stark effect which decreases the recombination efficiency.⁴ In order to suppress or to minimize the polarization effects, nonpolar, or semipolar growth orientations are extensively investigated.⁵⁻⁹ The nonpolar planes are those normal to (0001) planes, whereas semipolar ones are inclined by an angle between 0° and 90° relative to the basal planes [their indices are (hkil) with a nonzero *h* or *k* and nonzero *l* index]. When grown on substrates such as sapphire, the semipolar and nonpolar layers contains a high density of extended defects, mainly basal stacking faults (BSFs) and partial dislocations,^{7,10,11} which are detrimental for the optical properties. The propagation of such defects toward the surface is an obstacle to the regrowth of heterostructures with a sufficiently high crystalline quality for optical devices. In this work we have carried out an investigation of the semipolar (11 $\bar{2}$ 2) GaN grown on m-sapphire using the epitaxial lateral overgrowth (ELO).¹² Recently, it was shown that the density of defects reaching the surface can be significantly reduced by using an original process called asymmetric ELO.¹³ In the following, we report on the specific role of the prismatic stacking faults (PSFs) which are at the origin of the blocking process for the extended defects during the asymmetric ELO.

The growth of the semipolar layer by asymmetric ELO can be summarized in three steps [see Fig. 1(a) for a schematic representation]. First, a 2 μ m thick semipolar (11 $\bar{2}$ 2) GaN template is deposited by metal-organic vapor-phase epitaxy (MOVPE) on an m-plane (1 $\bar{1}$ 00) sapphire substrate. The in-plane epitaxial relationships are

$[1\bar{1}00]_{\text{GaN}} \parallel [11\bar{2}0]_{\text{sapphire}}$ and $[11\bar{2}3]_{\text{GaN}} \parallel [0001]_{\text{sapphire}}$.¹¹ Then, a 100 nm thick layer of SiO₂ is deposited by rf sputtering. SiO₂ stripes (7 μ m wide) are oriented along the [1 $\bar{1}$ 00] axis of GaN and separated by GaN windows (3 μ m wide). They are patterned by UV-lithography and chemical etching. The ELO was then performed in a single 2 in. wafer home-made MOVPE vertical reactor. Trimethylgallium and ammonia were used as precursors in a mixture of H₂/N₂ gas flows. The temperature was kept at 1080 °C during the entire process. In a first step, a GaN crystal seed was selectively deposited above the windows of the SiO₂ mask at a pressure of 20 kPa using a high V/III ratio (~3500). In a second step, the pressure was decreased to 10 kPa and the V/III ratio was drastically reduced down to 500. Growth was pursued until full coalescence of the films. This growth process was called asymmetric ELO.¹³ The layers after full coalescence are approximately 9 μ m thick. In these conditions, the growth rate along the +c direction is enhanced with eventually an overgrowth on top of adjacent stripes. An important consequence is that BSFs which propagate from the GaN windows are buried by the adjacent crystal along the coalescence front. We have carried out extensive observations of the coalescence boundary region [surrounded area on Fig. 1(a)] in order to identify the structure of defects that form and try to understand the mechanisms that govern the SFs blocking. For this investigation, conventional transmission electron microscopy (TEM) experiments were performed

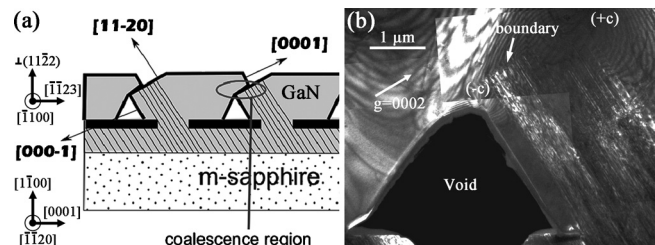


FIG. 1. (a) Schematic of a semipolar GaN layer grown by asymmetric ELO seen along the [1 $\bar{1}$ 00] zone axis (inclined lines are BSFs; the surrounded area indicates the investigated coalescence region). (b) A large view dark field micrograph ($g=0002$) around the coalescence area.

^{a)}Electronic mail: bertrand.lacroix@ensicaen.fr.

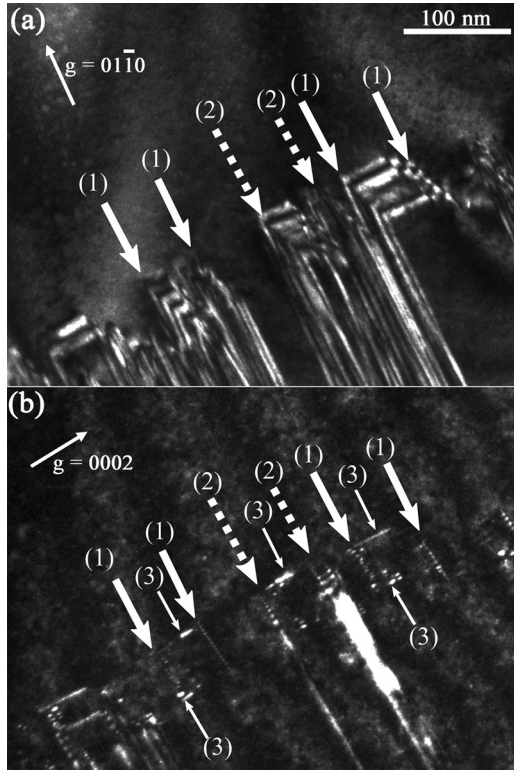


FIG. 2. Dark field micrographs close to the PSFs boundary region. Two configurations of intersection between BSFs and PSFs are marked [arrows (1) and (2)]. Partial dislocations bordering the PSFs are visible [arrows (3)]. (a) $\mathbf{g}=01\bar{1}0$: all SFs are in contrast except the E type, (b) $\mathbf{g}=0002$: all SFs are out of contrast; partial and connecting stair-rod dislocations with components along \mathbf{c} are visible.

with different diffraction vectors, \mathbf{g} , in weak beam conditions ($\mathbf{g}=0002$, $\mathbf{g}=11\bar{2}0$, and $\mathbf{g}=01\bar{1}0$). To this end, TEM cross-sections samples were prepared along the $[1\bar{1}00]$ direction by mechanical polishing using the tripod method down to thicknesses of a few microns. Subsequently, the electron transparency was achieved by argon ion milling at 5 kV using the GATAN precision ion polisher system at an incidence angle of 5° . TEM images were acquired in a JEOL 2010 microscope operated at 200 kV. Defects were identified as usual through the invisibility criterion which depends on the value of the scalar product $\mathbf{g}\cdot\mathbf{b}$ or $\mathbf{g}\cdot\mathbf{R}$ (where \mathbf{b} is the Burgers vector of dislocations and \mathbf{R} is the displacement vector of stacking faults): a dislocation is in contrast when $\mathbf{g}\cdot\mathbf{b} \neq 0$ and a SF is visible for $\mathbf{g}\cdot\mathbf{R} \neq \text{integer}$.

The use of asymmetric growth by mean of ELO inhibits significantly the propagation of the linear defects coming from the GaN template by comparison with previous observations concerning the symmetric growth.¹¹ They are stopped on the top of the voids, at a distance of about $3 \mu\text{m}$ from the interface with the template. As shown on the weak beam image acquired using $\mathbf{g}=0002$, close to the $[\bar{1}100]$ zone axis, a sharp boundary normal to the \mathbf{a} direction is clearly defined [Fig. 1(b)]. In this condition, BSFs are not visible and only partial dislocations that bound the BSFs are in contrast. By tilting the sample of about 30° around $[000\bar{1}]$ to reach the $[\bar{2}110]$ zone axis, the $\mathbf{g}=01\bar{1}0$ weak beam condition is obtained; we can now see that the BSFs [Fig. 2(a)] are terminated inside prismatic $\{11\bar{2}0\}$ planes, in the form of

TABLE I. Contrast of the SFs and partial dislocations in the wurtzite structure.

Type	Stacking Faults		$\mathbf{g}\cdot\mathbf{R}$	
	\mathbf{R}	$\mathbf{g}=01\bar{1}0$	$\mathbf{g}=0002$	
I1	$1/6[20\bar{2}3]$	$1/3$	1	
I2	$1/3[10\bar{1}0]$	$1/3$	0	
E	$1/2[0001]$	0	1	
D	$1/2[10\bar{1}1]$	$1/2$	1	
A	$1/6[20\bar{2}3]$	$1/3$	1	

Type	Partial dislocations		
	\mathbf{b}	$\mathbf{g}=01\bar{1}0$	$\mathbf{g}=0002$
Frank-Shockley	$1/6[20\bar{2}3]$	$1/3$	1
Shockley	$1/3[10\bar{1}0]$	$1/3$	0
Frank	$1/2[0001]$	0	1

inclined sections exhibiting fringes. Such defects have been first identified in ZnS (Refs. 14 and 15) and later in GaN.¹⁶ They have been shown to correspond to a PSF with two possible atomic configurations (Drum-D: $1/2[10\bar{1}1]$ and Amelinckx-A: $1/6[20\bar{2}3]$).¹⁷ The relative stability of the two atomic configurations have also been reported subsequent to investigation using a combination of atomistic modeling and high resolution TEM.^{18,19} In this instance, they are visible along the coalescence boundary as shown by the corresponding fringes in Fig. 2(a) recorded using $\mathbf{g}=01\bar{1}0$. They have various sizes and they can reach a lateral extension of 45 nm.

By examining in detail a specific area with $\mathbf{g}=0002$ [Fig. 2(b)], we can notice the presence of fine and small parallel lines all along the coalescence boundary. They are located at the border of the PSFs as can be seen by comparing Figs. 2(a) and 2(b) [see arrows (1) and (2)]. These lines correspond to partial dislocations which were generated at the top of BSFs coming from the template when the PSFs formed. In GaN, three types of BSFs (I1, I2, and E) and two types of PSFs (D and A) may form (Table I). Therefore, six configurations are possible in these interactions, they may give rise or not to stair-rod dislocations as shown in Table II.

As can be seen on Fig. 2, two configurations of interactions between the basal and prismatic SFs are visible. In the first [arrows (1)], stair-rods are visible with $\mathbf{g}=0002$ in the continuation of the BSFs (visible with $\mathbf{g}=01\bar{1}0$), whereas partial dislocations that border the BSFs are not visible. Therefore, using Table I, we can conclude that such BSFs are

TABLE II. Contrast of the stair-rod dislocations.

BSF-PSF connection	\mathbf{b}	$\mathbf{g}\cdot\mathbf{b}$	
		$\mathbf{g}=01\bar{1}0$	$\mathbf{g}=0002$
I1-D	$1/6[10\bar{1}0]$	$1/6$	0
I1-A	no
E-D	$1/2[10\bar{1}0]$	$1/2$	0
E-A	$1/3[10\bar{1}0]$	$2/3$	0
I2-D	$1/6[10\bar{1}3]$	$1/6$	1
I2-A	$1/2[0001]$	0	1

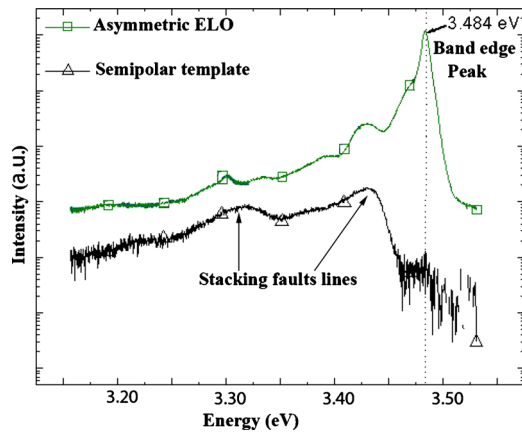


FIG. 3. (Color online) PL emissions from a semipolar GaN template and the asymmetric ELO layer.

I2 (bordered by Shockley partial dislocations: $1/3(10\bar{1}0)$). As shown in Table II, only two configurations can give rise to visible stair-rod dislocations using $\mathbf{g}=0002$: they may correspond to interaction of I2 BSFs with Drum (D) or with Amelinckx (A) PSFs. However, using $\mathbf{g}=01\bar{1}0$, no intensity reinforcement is observed at the crossover of these BSFs and the PSFs which tends to show that the interaction corresponds to a switching between an I2-BSF and an A-PSF, through the formation of an E ($1/2[0001]$) partial dislocation. In the second configuration [arrows (2)], partial dislocations are in contrast using $\mathbf{g}=0002$ [Fig. 2(b)] at the border of the BSFs which are in contrast in Fig. 2(a). Therefore, they are Frank–Shockley dislocations (Table I), which means that the related BSFs are of I1-type (the E BSFs are not visible with $\mathbf{g}=01\bar{1}0$). However, such images do not help to determine the configuration of the PSF, indeed, the $1/6[10\bar{1}0]$ stair rod dislocation which should connect the I1-BSF to the D-PSF is out of contrast in Fig. 2(b), whereas the A-PSF keeps the same displacement vector when folding from the basal to the prismatic plane. As indicated by the arrows (3), we also notice the presence of defects inside the prismatic planes which are in contrast for $\mathbf{g}=0002$, they are seen at upper and bottom of the PSFs. This is a clear evidence that the PSFs are also terminated at short distances during the formation of this boundary (the Burgers vectors correspond to that of the displacement vectors of the PSFs, A: $1/6\langle 20\bar{2}3 \rangle$ and D: $1/2[10\bar{1}1]$, respectively, indeed the two are in contrast with $\mathbf{g}=0002$).

This structural investigations of a semipolar ($11\bar{2}2$) GaN layer shows that the use of asymmetric growth conditions is efficient to stop the propagation of the BSFs arising from the GaN aperture between the masks. These extended defects are blocked in the bulk, in the vicinity of the coalescence region between two subsequent apertures, thanks to the nondefective laterally grown material over the mask and this enables to obtain a defect-free surface layer. The blocking process of the BSFs is mediated by the formation of PSFs in the $\{11\bar{2}0\}$

lattice planes. These PSFs exhibit both Drum configuration and Amelinckx configuration, which is less energetically favorable as reported in the literature.^{19,20} The formation of these two types of PSFs along a well defined boundary seems to be related to the growth anisotropy. Indeed, due to the significant enhancement of the growth rate along the $+c$ direction, high stress fields may be localized close to the coalescence region, when the $(-c)$ and $(+c)$ facets meet, making the folding of SFs into the prismatic plane easier.

By comparison, a GaN template layer grown without ELO contains a higher density of extended defects that propagate to the surface.¹¹ The use of asymmetric ELO leads to a good crystalline quality of the whole GaN surface layer, considerably improving the optical properties of the material. As shown in Fig. 3, the GaN band edge peak, which is almost not visible in photoluminescence (PL) spectrum from the templates is increased by more than four orders of magnitude in asymmetric ELO layers. Moreover, one can also notice a decrease in emission intensity at 3.42 and 3.29 eV which correspond to the luminescence from the BSFs and partial dislocations.

The National Research Agency (ANR) under Contract No. BLAN08-1_323691-COSNI and “la Région Basse Normandie” are gratefully acknowledged for their support to this research work.

¹S. Nakamura, G. Fasol, and S. J. Pearton, *The Blue Laser Diode* (Springer, New York, 2000).

²F. Bernardini, V. Fiorentini, and D. Vanderbilt, *Phys. Rev. B* **56**, R10024 (1997).

³F. Bernardini and V. Fiorentini, *Phys. Status Solidi B* **216**, 391 (1999).

⁴V. Fiorentini, F. Bernardini, F. Della Sala, A. Di Carlo, and P. Lugli, *Phys. Rev. B* **60**, 8849 (1999).

⁵P. Waltereit, O. Brandt, A. Trampert, H. Grahm, J. Menniger, M. Ramsteiner, M. Reiche, and K. Ploog, *Nature (London)* **406**, 865 (2000).

⁶L. Lahourcade, J. Renard, B. Gayral, E. Monroy, M. P. Chauvat, and P. Ruterana, *J. Appl. Phys.* **103**, 093514 (2008).

⁷M. D. Craven, S. H. Lim, F. Wu, J. S. Speck, and S. P. DenBaars, *Appl. Phys. Lett.* **81**, 469 (2002).

⁸L. Lahourcade, E. Bellet-Amalric, E. Monroy, M. Abouzaid, and P. Ruterana, *Appl. Phys. Lett.* **90**, 131909 (2007).

⁹T. J. Baker, B. A. Haskell, F. Wu, J. S. Speck, and S. Nakamura, *Jpn. J. Appl. Phys., Part 2* **45**, L154 (2006).

¹⁰D. N. Zakharov, Z. Liliental-Weber, B. Wagner, Z. J. Reitmeier, E. A. Preble, and R. F. Davis, *Phys. Rev. B* **71**, 235334 (2005).

¹¹Y. A. R. Dasilva, M. P. Chauvat, P. Ruterana, L. Lahourcade, E. Monroy, and G. Nataf, *J. Phys.: Condens. Matter* **22**, 355802 (2010).

¹²P. Gibart, *Rep. Prog. Phys.* **67**, 667 (2004).

¹³N. Kriouche, P. Vennéguès, M. Nemoz, G. Nataf, and P. de Mierry, *J. Cryst. Growth* **312**, 2625 (2010).

¹⁴H. Blank, P. Delavignette, R. Gevers, and S. Amelinckx, *Phys. Status Solidi B* **7**, 747 (1964).

¹⁵C. M. Drum, *Philos. Mag.* **11**, 313 (1965).

¹⁶P. Vermaut, P. Ruterana, G. Nouet, and H. Morkoç, *Philos. Mag. A* **75**, 239 (1997).

¹⁷P. Vermaut, G. Nouet, and P. Ruterana, *Appl. Phys. Lett.* **74**, 694 (1999).

¹⁸N. Aïchoune, V. Potin, P. Ruterana, A. Hairie, G. Nouet, and E. Paumier, *Comput. Mater. Sci.* **17**, 380 (2000).

¹⁹P. Ruterana, B. Barbaray, A. Béré, P. Vermaut, A. Hairie, E. Paumier, G. Nouet, A. Salvador, A. Botchkarev, and H. Morkoç, *Phys. Rev. B* **59**, 15917 (1999).

²⁰J. E. Northrup, *Appl. Phys. Lett.* **72**, 2316 (1998).